Journal of Fluids and Structures 48 (2014) 487–496

Contents lists available at ScienceDirect

Journal of Fluids and Structures

journal homepage: www.elsevier.com/locate/jfs

Experimental study of the aerodynamic characteristics of a low-aspect-ratio flat plate array in a configuration of interest for a tidal energy converter

F. Fedoul, L. Parras, C. del Pino, R. Fernandez-Feria*

E. T. S. Ingeniería Industrial, Universidad de Málaga, Dr Ortiz Ramos s/n, 29071 Málaga, Spain

ARTICLE INFO

Article history:
Received 7 March 2013
Accepted 13 April 2014
Available online 10 May 2014

Keywords:
Cascade
Tidal energy converter
Aerodynamics

ABSTRACT

Wind tunnel experiments were conducted for the flow around a single flat plate and through an array of three parallel flat plates at different angles of incidence to compare their lift and drag coefficients for several values of the Reynolds number around 10^5 and for three aspect ratio values. The selected cascade configuration is of interest for a particular type of tidal hydrokinetic energy converter. The main differences in the lift and drag forces are discussed, finding that for a plate in a cascade the maximum lift coefficient takes place at a quite different angle of attack, depending on the aspect ratio. The optimal conditions for extracting power from a tidal current are analyzed.

1. Introduction

The study of the flow through cascades (or lattices of airfoils) is of great practical interest for the aerodynamics of turbines and compressors, and much theoretical and experimental effort was expended, mainly during the development of the axial turbines and compressors in the first half of the 20th Century, to characterize the aerodynamic forces exerted on the blades of a cascade (see, e.g. Hawthorne, 1964). As a consequence, a large amount of experimental data for the aerodynamic characteristics of very different types of cascades, many of them obtained in specially designed wind tunnels, have been accumulated over the years, both for low speed (incompressible) and high speed (compressible) flows (see, e.g. Gostelow, 1984, Chapters 2 and 4, Hodson and Howell, 2005, and references therein). However, no experimental data exist, to the best of our knowledge, for the aerodynamic characteristics of a cascade of low-aspect-ratio blades at moderate or relatively low Reynolds numbers, being perhaps the most similar configuration for which there exists experimental data that of a vertical axis wind turbine (e.g. McLaren et al., 2012). The incompressible flow through such a cascade is of current interest for a particular device to extract kinetic energy from tidal currents, consisting of a cascade of underwater sails or blades that travel carried by the tidal current in a given direction, which in turn drive an electric generator ('Tidal Sails AS', 2012). It is also of basic aerodynamics interest to find out how the lift and drag forces on a blade in a cascade are affected by the adjacent ones, in relation to the forces on an isolated blade, when the aspect ratio is varied for moderate and low Reynolds numbers. This problem is even more topical now because of the growing interest in the aerodynamics of low-aspect-ratio wings at low Reynolds numbers aimed at the development of fixed-wing micro aerial vehicles (e.g. Mueller et al., 2007), so that new experimental data for low-aspect-ratio wing aerodynamics at low Reynolds numbers are becoming

* Corresponding author.
E-mail address: ramon.fernandez@uma.es (R. Fernandez-Feria).

http://dx.doi.org/10.1016/j.jfluidstructs.2014.04.001
0889-9746/

available in recent years (Pelletier and Mueller, 2000; Torres and Mueller, 2004), complementing older experimental data aimed at the understanding of the enhanced lift in short span rectangular wings (e.g. Winter, 1936).

We consider in the present work a cascade of flat plates with different values of the aspect ratio (AR), measuring in a wind tunnel the lift and drag forces on a plate in the cascade for increasing values of the angle of attack (α) and for different Reynolds (Re) numbers (these nondimensional quantities are defined in the next section). The aerodynamic forces are compared with those on an isolated flat plate for the same values of AR, α and Re. The simplicity of flat rectangular airfoils has also been the reason for its selection as a reference blade in the above-mentioned works for low-aspect-ratio wing aerodynamics (Pelletier and Mueller, 2000; Torres and Mueller, 2004), whose experimental results will be used here to check our single flat plate results and thus to validate the experimental measurements. In addition, the blades in the actual arrays used in the device for extracting hydrokinetic tidal energy that motivates the present work are symmetrical thin airfoils ('Tidal Sails AS', 2012) that can be assumed to be rectangular flat plates in a first approximation. Of course, subsequent experimental studies on the aerodynamics of these devices have to take into account the effect of the blade profiles.

In the experiments reported in the present work we use flat plates with three different values of the AR, namely 1, 2 and 6, and several values of the Reynolds number around 10^5. Actually, we take advantage of the flow symmetry about the middle plane and consider flat plates anchored in the base of the wind tunnel test section with values of the semispan aspect ratio (sAR) of 0.5, 1, and 3. These values of the aspect ratio are within the range of interest in the mentioned tidal energy converters, and coincide with some of the ones considered by Pelletier and Mueller (2000) for a single flat plate, used to validate our experimental results.

In relation to the cascade configuration, we used an array of three stationary flat plates forming an angle of 45° with the wind tunnel flow direction in the test section, and measure the aerodynamic forces on the central plate in the cascade as the angle of attack α is varied for different values of sAR and Re. This configuration corresponds, for instance, to a cascade moving perpendicularly to the current with the same speed as the current (see the next section). Some other arrays could have been tested, but this seems to be one of the optimal configurations in actual tidal current devices (Mayorga, 2012). A similar configuration, but for the aerodynamic study of a linear oscillating cascade, was used by Buffum and Fleeter (1991).

2. Experimental set-up

For the experiments we used a low-speed closed circuit wind tunnel with a test section of $1 \times 1\ \mathrm{m}^2$ cross section. Either a rectangular flat plate or an array of three of them was mounted in the test section of the wind tunnel (see Fig. 1, where it is shown the array of three plates). The main objective of this experimental study was to compare these two configurations in terms of the aerodynamical forces for one (isolated or central) plate mounted on a platform force balance. However, to check that the extent of the cascade with just three blades was enough for obtaining relevant results, we also used an array of five flat plates. No significant differences for the forces exerted by the flow on the central plate in the cascade were observed (see Section 4).

The plates were made of steel with 2 mm thickness and 15 cm chord length (i.e., a thickness-to-chord ratio of 1.33%). Several values of the aspect ratio were used. The leading and trailing edges of these steel plates were both tapered on a length of about 2.5 times its thickness, and identical plates were used in both the single plate configuration and the array of three plates, so that the effect of the adjacent plates in the cascade on the aerodynamic characteristics of a plate could be analyzed.

The array of three flat plates was mounted with an angle of 45° in relation to the wind tunnel current (see Fig. 1). As commented on above, this configuration corresponds to a cascade moving perpendicularly to a tidal or river current with the same speed as the current (see Fig. 2, where the cascade speed U is equal to the current speed V). The wind tunnel speed $W = \sqrt{V^2 + U^2} = \sqrt{2}V$ corresponds to the relative air velocity to the plates in a reference frame moving with the cascade. We used this speed W and the chord length c ($=15$ cm) as the reference velocity and length scale, respectively, to define the Reynolds number,

$$\mathrm{Re} = \frac{Wc}{\nu}, \tag{1}$$

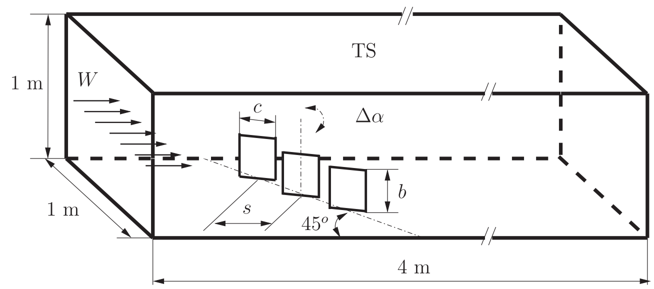

Fig. 1. Sketch of the wind tunnel test section with the array of three flat plates.

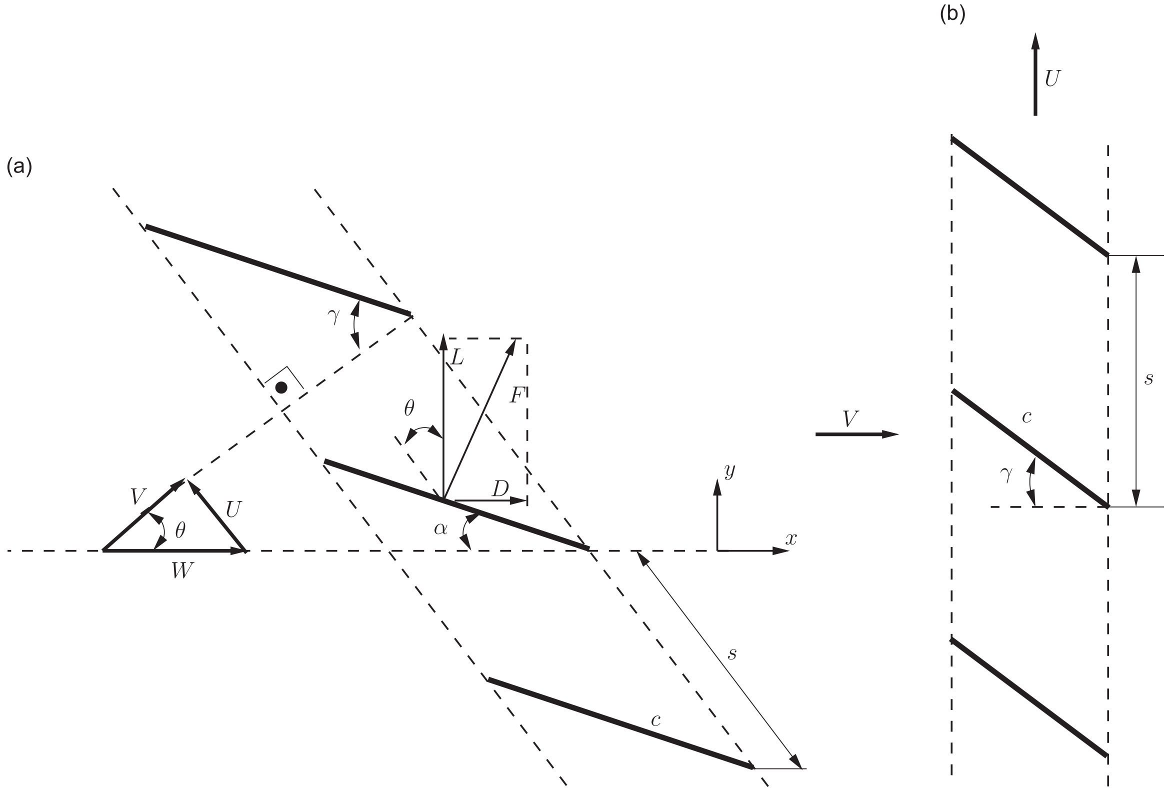

Fig. 2. Sketch of the plan view of the array of three flat plates in the wind tunnel reference frame with current velocity W in the x-direction (a), corresponding to a cascade moving with velocity U perpendicularly to a current with velocity V (b). In the present study $U=V$ (i.e., $\theta=45^\circ$) and $s=c$.

where ν is the kinematic viscosity. The three plates were mounted together with a separation s between them in an articulated aluminium frame that allowed us to change simultaneously the angle of attack α of the plates. We chose $s=c$, i.e. a solidity $\sigma \equiv c/s$ of unity, which is the most effective value for enhancing the lift coefficient of a plate in a cascade in relation to an isolated plate according to the two-dimensional potential flow theory of cascades (Weinig, 1964). In our experiments, we varied the angle of attack α, the Reynolds number through the speed W, and the aspect ratio of the plates.

Actually, as commented on in the Introduction, we used a semispan aspect ratio sAR ($=b/c$ in Fig. 1) to characterize the different aspect ratios of the plates, because we mounted the single plate, or the array of them, on the force balance perpendicularly to the bottom surface of the wind tunnel test section, so that this surface acted as a symmetry plane in the flow through the plates. Fig. 3 shows a schematic of the balance set-up located below the bottom surface of the wind tunnel test section when the array of flat plates is mounted on it. A three-component force sensor was used to measure the lift and drag forces (y and x components of the force F, see Fig. 2) on either an isolated plate or the central plate in an array of three plates. The maximum force that could be measured with the sensor in these directions was 32 N, whereas the minimum measurable lift and drag forces were about 0.01 N. The force sensor was calibrated previously to the series of experiments reported here using a standard dynamometer, showing a linear behavior in the three spatial axes and an error lower than 1% for the whole measurement range. We also calibrated the wind tunnel velocity W, which was recorded through a hot wire anemometer during the experiments, using independent Laser Doppler Anemometry measurements across the wind tunnel test section. The free stream turbulence intensity was less than 3% for the range of velocities used in this work.

3. Experimental procedures and validation

We used three values of the semispan aspect ratio, sAR=0.5, 1, and 3, for both the isolated plate and the array of three plates, and four values of the stream velocities W, corresponding to Reynolds numbers $Re=4.4\times 10^4$, 8×10^4, 1.5×10^5, and 2.25×10^5. Both the stream velocity and the temperature were continuously measured to control the Reynolds number.

For each aspect ratio of the single plate or the set of three plates, and for each Reynolds number, we measured the x and y force components (D and L) for values of the angle of attack α varying between -35° and $+35^\circ$. The data acquisition (of the force components, stream velocity and temperature) and the variation of the angle of attack were both controlled by a PC through the software LABVIEW®. Since the force sensor was attached to the plate, its measurement axis did not coincide exactly with the wind tunnel axis. Thus, to get the initial angle of attack $\alpha=0^\circ$, we first rotated the plates' small angles around its parallel position to the wind tunnel axis and measured the force components looking for the minimum absolute

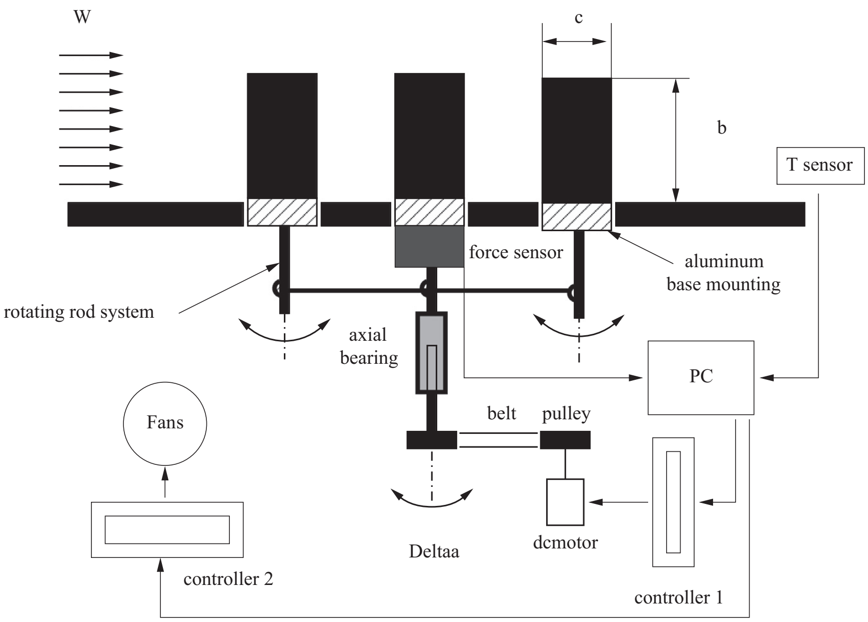

Fig. 3. Sketch of the experimental set-up with the balance arrangement and the array of three plates in the test section.

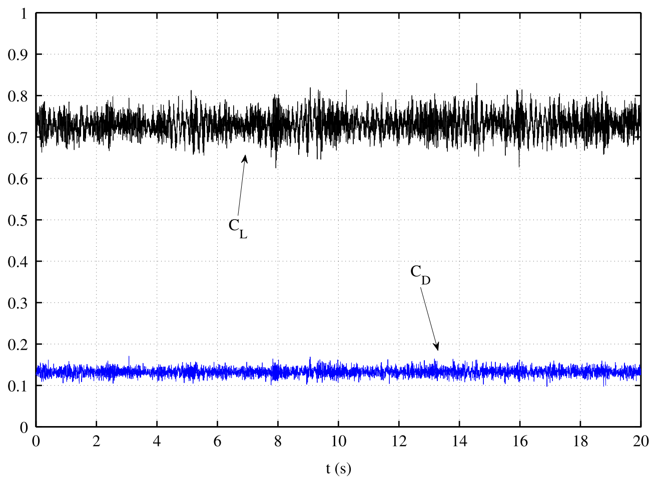

Fig. 4. Typical recording of the nondimensional force components C_D and C_L for an isolated plate with $\mathrm{Re}=1.5\times10^5$ and $\alpha=10^\circ$.

force. Once the null angle of attack was thus selected, we increased it by steps of 2.5° until $\alpha=+35^\circ$, and then decreased it with the same step until $\alpha=-35^\circ$ was reached. No hysteresis was observed in any of the force measurements.

We recorded the two components of the force for each angle of attack during 20 s at a rate of 2600 Hz (i.e., 52 000 measurements), which allowed us to obtain reliable mean values of the forces and their fluctuation characteristics. These results were not affected by increasing the acquisition time. Fig. 4 shows a typical record of the nondimensional force components for a single plate, where the drag and lift coefficients are defined as

$$C_D=\frac{D}{\frac{1}{2}\rho W^2 A},\quad C_L=\frac{L}{\frac{1}{2}\rho W^2 A}, \tag{2}$$

ρ being the air density, $A=cb$, and the semispan length $b=(\mathrm{sAR})c$. During each measurement test we also recorded the stream velocity W and the temperature, so that their fluctuations were also taken into account in C_D, C_L, and Re.

The oscillations in the coefficients C_D and C_L were not only due to uncertainties in the measurement process, but also to physical fluctuations caused by vortex shedding, which was particularly important for a single plate when the angle of attack $|\alpha|$ was high enough. For the flow through the cascade, these fluctuations by vortex shedding were significantly smaller than for a single plate in all the range of α considered.

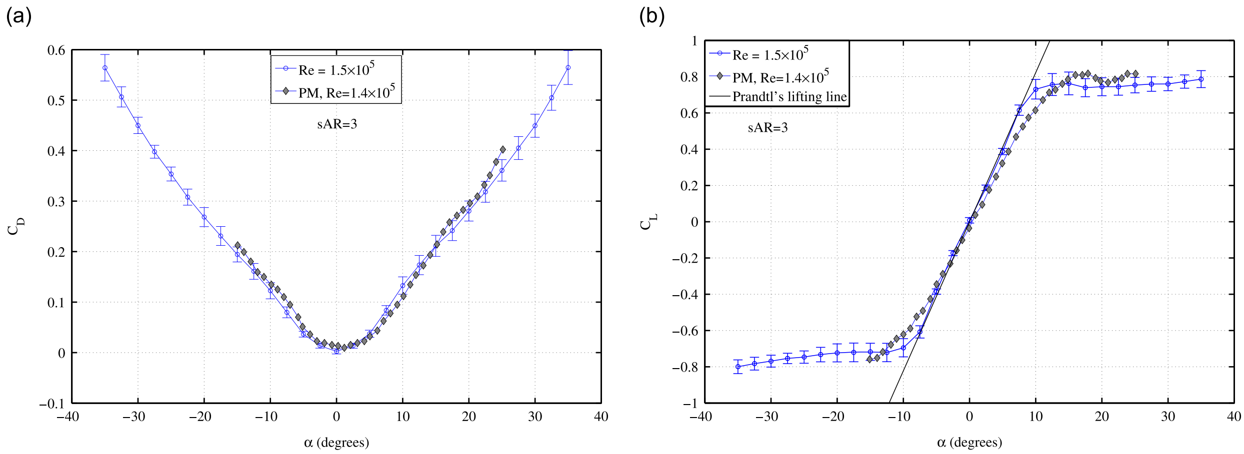

Fig. 5. Comparison between our measured values of $C_D(\alpha)$ (a) and $C_L(\alpha)$ (b) for an isolated plate with sAR=3 and for Re=1.5×10^5 with the experimental results reported by Pelletier and Mueller (2000) (PM in the legend) for the same sAR and a quite similar Re. The result from Prandtl's lifting line theory for symmetric, rectangular wing with no twist and finite span, $C_L \simeq m\alpha$, with $m = 2\pi/[1+1/(\text{sAR})]$ (e.g. Keuthe and Chow, 1997) is also included in (b) for reference sake.

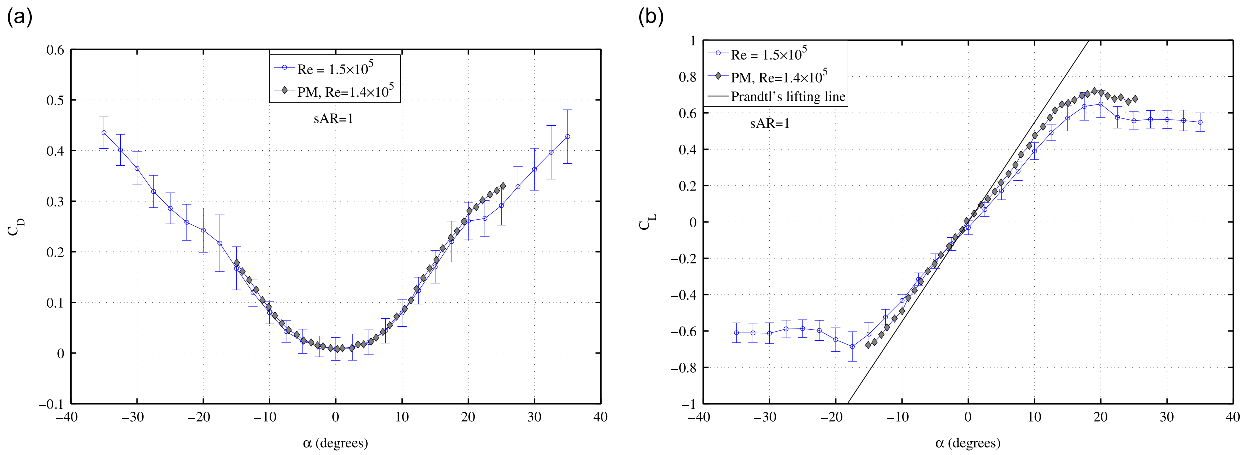

Fig. 6. As in Fig. 5, but for sAR=1.

To validate our experimental results for C_D and C_L we made a comparison, for the case of a single plate, with the results reported by Pelletier and Mueller (2000) for several values of sAR and Re. Figs. 5 and 6 show this comparison for $C_D(\alpha)$ and $C_L(\alpha)$ when sAR=3 and 1, respectively. The error bars in these figures correspond to the standard deviation of the fluctuations. It is observed that the mean results agree fairly well with those obtained by Pelletier and Mueller. Note that the Reynolds number is slightly different and that the flat plates used by these authors had different geometries of the leading and trailing edges. Although the effect of the leading edge is beyond the scope of this study, it may explain the differences observed in Fig. 6(a) for $\alpha > 20^\circ$. Some other cases for a single plate were compared with a similar good agreement.

4. Results and discussion

Once our results for a single plate were validated, we compared them with those for a plate in a cascade for all the different values of Re and sAR considered in this work. Fig. 7 shows this comparison for a typical case with sAR=3. We show the results obtained with an array of 3 and 5 flat plates. Since there are no significant differences between the results obtained from these two arrays, it is concluded that there is no relevant tunnel blockage effects and that 3 blades are a sufficient cascade extent. Therefore, all the results reported below for a cascade are obtained with an array of three plates.

The first main feature that results from this comparison is that the symmetry of the mean values of $C_D(\alpha)$ and the antisymmetry of the mean values of $C_L(\alpha)$ in relation to $\alpha=0$ for an isolated plate are both obviously lost for a plate in the cascade. Since in the present cascade configuration only the region $\alpha \geq 0$ is relevant for the practical application, the results for negative values of α will not be reported nor plotted in the subsequent figures. It is also observed in Fig. 7 that both C_D

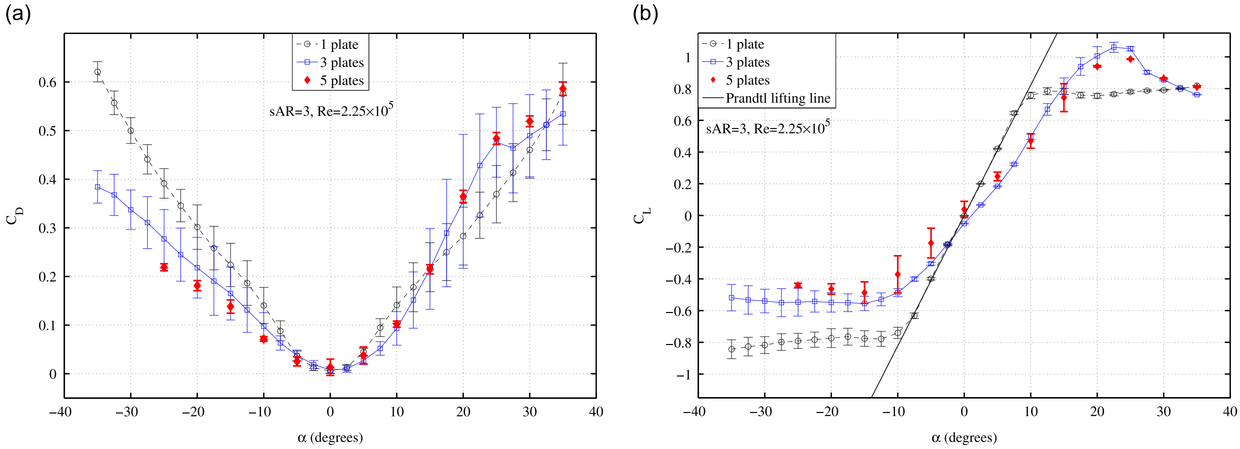

Fig. 7. Comparison between $C_D(\alpha)$ (a) and $C_L(\alpha)$ (b) for a single plate and for the central plate in a cascade of three and five plates when Re = 2.25×10^5 and sAR = 3. The result from Prandtl's lifting line theory for symmetric, rectangular wing with no twist and finite span (see caption of Fig. 5) is also included in (b) for reference sake.

and C_L for a plate in the cascade are smaller than their single plate counterparts as α increases from zero ($\alpha \geq 0$). The curves then cross, at different values of α, so that C_D and C_L in a cascade become larger than in a single plate in a certain region of values of α. Finally, the curves cross again so that C_D and C_L are quite similar to each other in both cases for values of α close to the largest one reported here. Particularly significant is the maximum value of C_L for a plate in the cascade, which occurs for a value of α well above the one for which the single plate becomes stalled. In the case of Fig. 7, the separation of the flow in a single plate occurs at $\alpha \approx 10^\circ$, so that the mean value of C_L remains practically constant above this α. But, for a plate in the cascade, C_L keeps increasing, owing to the streaming effect produced by the adjacent plates that delays the flow separation, till it reaches a maximum value at $\alpha \approx 25^o$ and then decays when the plate in the cascade becomes also stalled. This is illustrated in the flow visualizations of Fig. 8, where it is shown the final results of post-processing the temporal evolutions of 500 instantaneous frames using smoke as a particle tracer method. The figure shows the visualizations of the flow around one plate and through the array of three plates for the Reynolds number of Fig. 7 and for two values of α: 10° and 20°. For 20° the single plate is stalled, with the flow over the plate completely separated, while the flow around the central plate in the cascade remains attached to the plate. This also explains why the lift curve slope is smaller in the cascade, since the induced downwash angle is increased in relation to a single plate.

The same features are observed for all the Reynolds numbers considered in this work when sAR = 3 (see Figs. 9–12, where only the mean values of C_D and C_L for $\alpha \geq 0$ are plotted). Also when sAR = 1, but with a less pronounced maximum of $C_L(\alpha)$ for a plate in the cascade, which takes place at larger values of α than for sAR = 3 (for $\alpha \approx 30^\circ$). However, for the smallest value of the aspect ratio (sAR = 0.5), this behavior for $C_L(\alpha)$ is not observed. Actually, for sAR = 0.5, the functions $C_D(\alpha)$ and $C_L(\alpha)$ for a single plate and for a plate in the cascade are all quite similar, which is a consequence of the fact that the influence of the adjacent plates in the cascade becomes negligible as the aspect ratio decreases (for a given separation between plates or solidity of the cascade). Note, however, that no results are plotted in Figs. 11 and 12 for sAR = 0.5 because for the lower Reynolds numbers considered the forces on the smallest plate (sAR = 0.5) were below the minimum value that can accurately be measured by the force sensor (for the lowest Re = 4.4×10^4, plotted in Fig. 12, not even the case with sAR = 1 could be measured with sufficient accuracy).

A relevant magnitude for the particular cascade configuration considered in this work is the effective power extracted to the actual current with speed V when the cascade moves with speed U (see Fig. 2), which is proportional to

$$P_U = (L\cos\theta - D\sin\theta)U = \frac{\sqrt{2}}{2}(L-D)U. \tag{3}$$

It is convenient to define the power coefficient

$$C_P \equiv \frac{P_U}{\frac{1}{2}\rho V^3 A} = \sqrt{2}(C_L - C_D). \tag{4}$$

Fig. 13 compares $C_P(\alpha)$ for a plate in the cascade with that for a single plate in the different cases considered. In both configurations, C_P reaches a maximum value $C_{P,max}$ for an angle of attack $\alpha = \alpha_{max}$ that depends on sAR, and, to a lesser extent, on Re. Only for the largest aspect ratio sAR = 3 are the maximum values of C_P for a plate in the cascade larger than those for an isolated plate [Fig. 13(a)], but the differences are quite small. However, these maxima take place at values of α that are almost twice than for a single plate. As sAR decreases, $C_{P,max}$ for a cascade becomes smaller than for a single plate and the values of α_{max} approach each other, as it is clear for sAR = 0.5 in Fig. 13(c). This behavior of $C_P(\alpha)$ for a plate in the cascade when sAR is not too small contrasts with that of $C_L(\alpha)$, which has a pronounced maximum in relation to a single

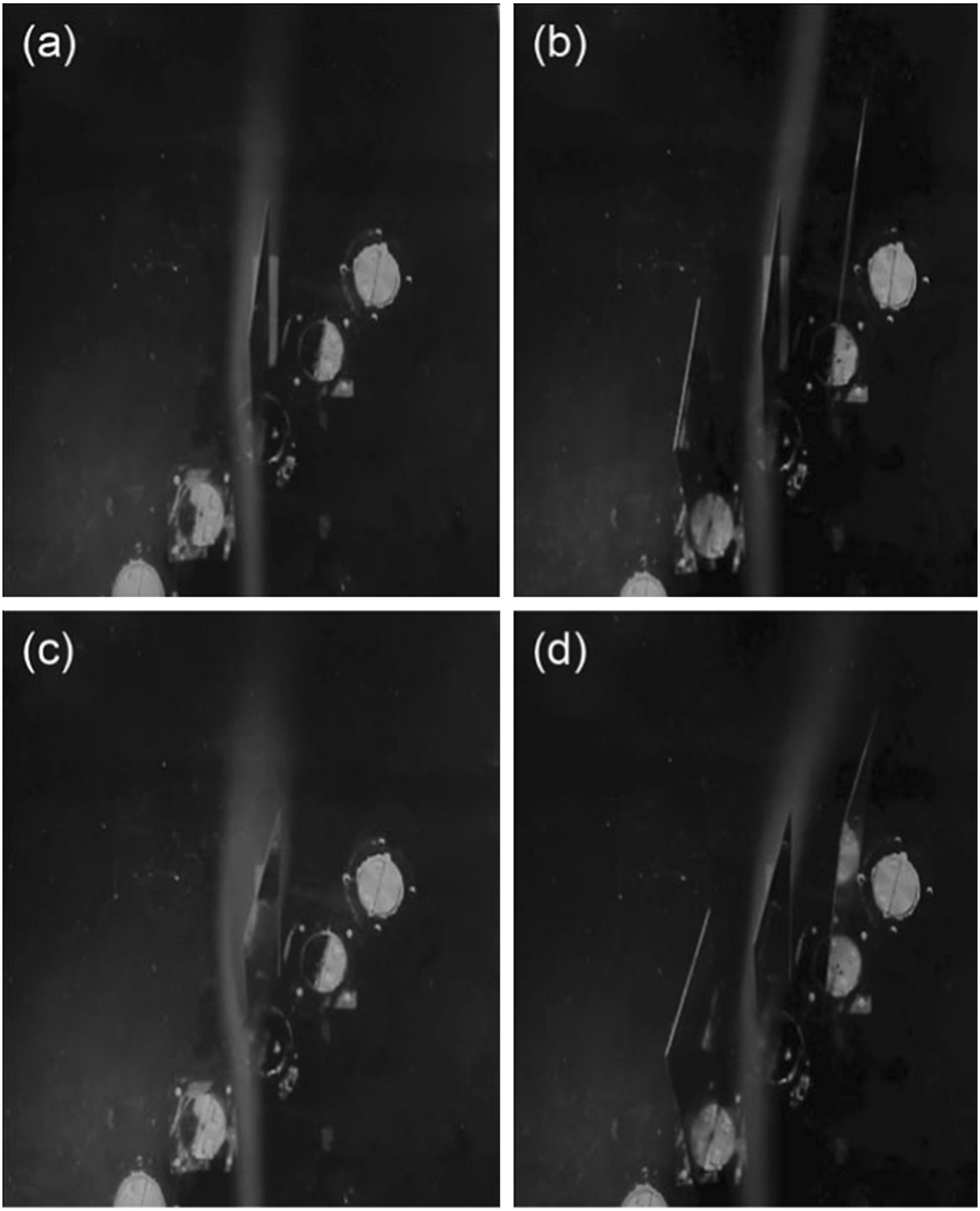

Fig. 8. Smoke flow visualizations for the same Re and aspect ratio of Fig. 7 for $\alpha = 10^{\circ}$ [(a) and (b)] and $\alpha = 20^{\circ}$ [(c) and (d)], for a single plate [(a) and (c)] and for an array of three plates [(b) and (d)].

plate for all the Reynolds numbers considered. It is a consequence of the fact that C_D for the plate in the cascade becomes also significantly larger than for a single plate for the values of α where C_L reaches its maximum (see Figs. 9–12; also Fig. 7, where this feature is quite clear). Thus the enhancement of the lift coefficient for a plate in a cascade in relation to an isolated plate for sufficiently high values of the angle of attack, which is specially relevant when the aspect ratio is not too

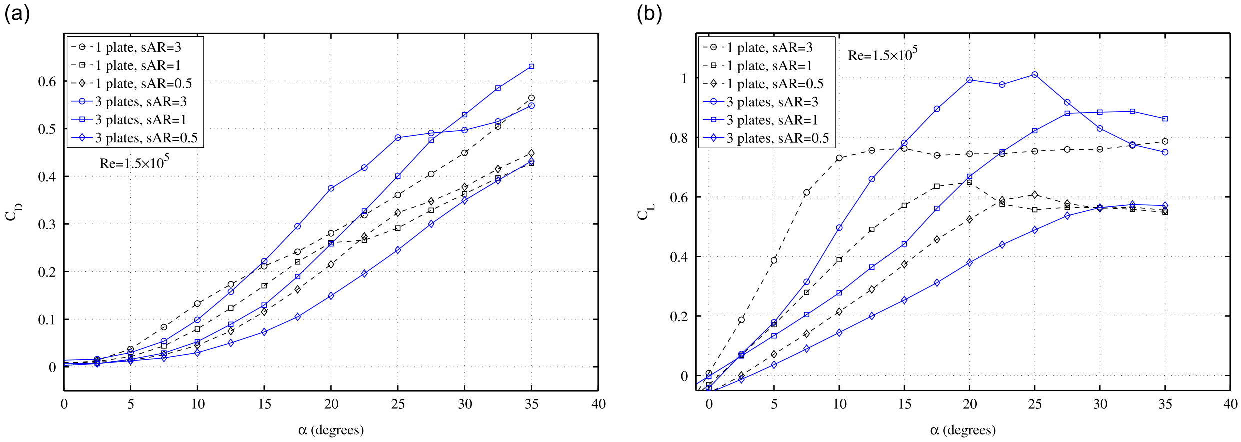

Fig. 9. Comparison between $C_D(\alpha)$ (a) and $C_L(\alpha)$ (b) for a single plate and for the central plate in a cascade of three plates when $\mathrm{Re}=2.25\times10^5$ and for different values of sAR.

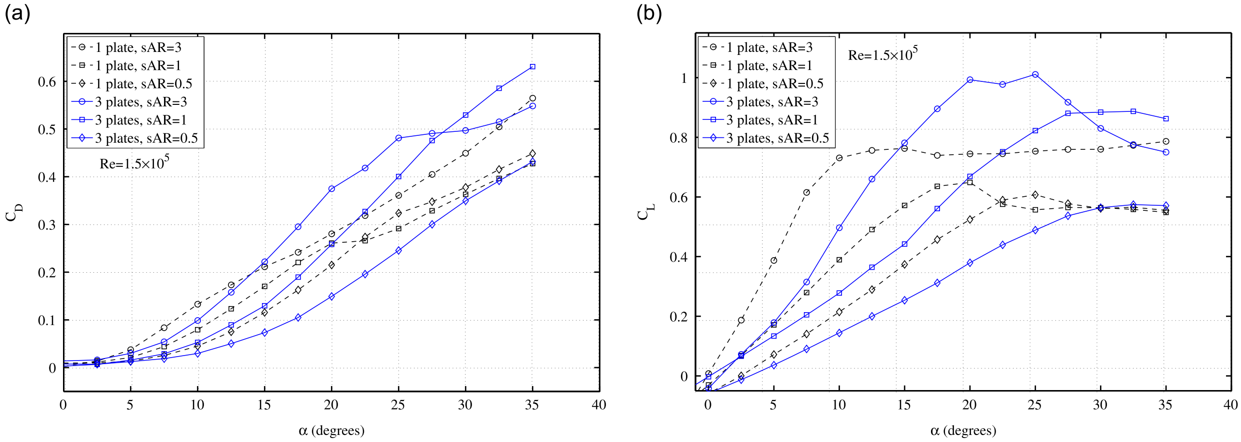

Fig. 10. As in Fig. 9, but for $\mathrm{Re}=1.5\times10^5$.

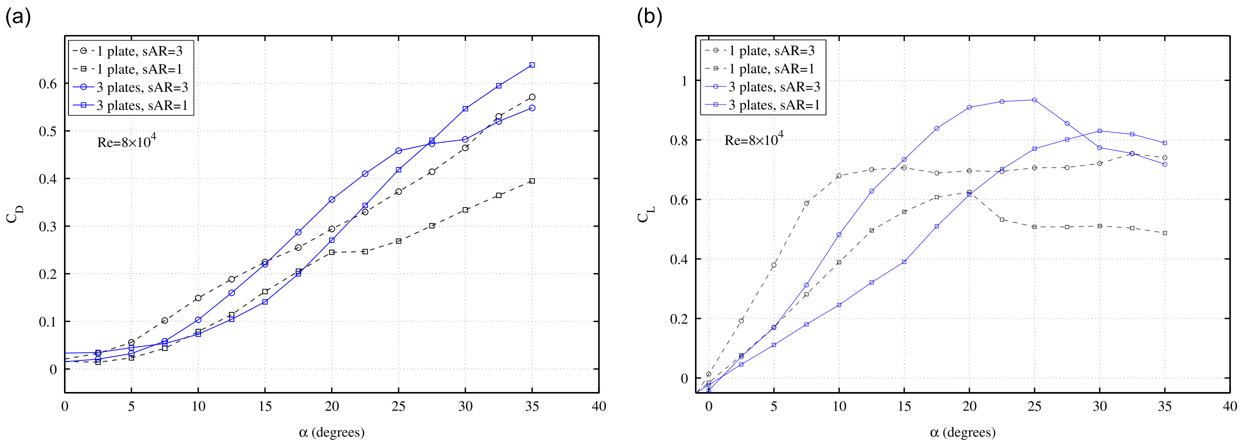

Fig. 11. As in Fig. 9, but for $\mathrm{Re}=8\times10^4$.

small (for sAR=3 and sAR=1 in the present study), does not produce a significant power coefficient enhancement in the present configuration of interest for a tidal current converter because the drag coefficient is also increased for the corresponding values of the angle of attack.

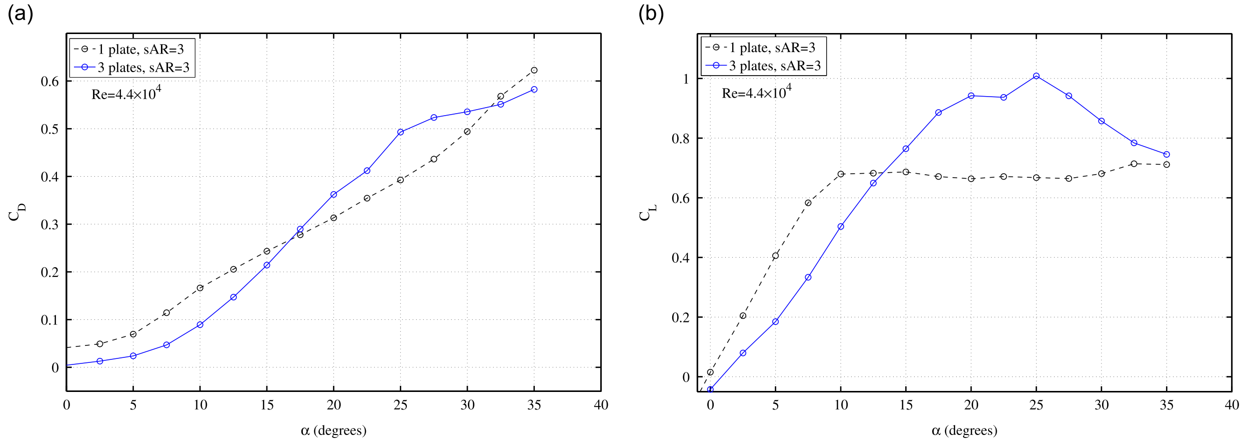

Fig. 12. As in Fig. 9, but for Re $=4.4\times10^4$.

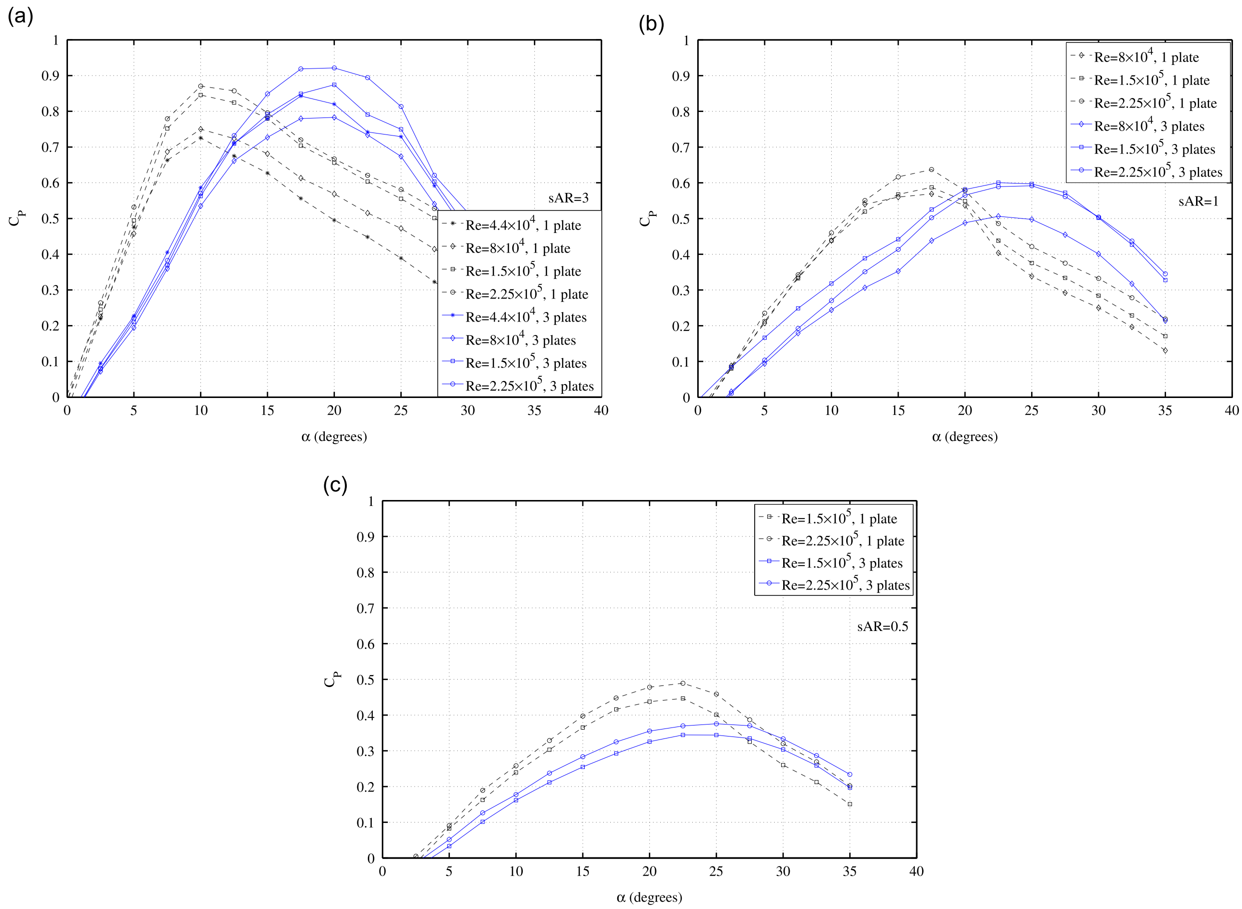

Fig. 13. Comparison between $C_P(\alpha)$ for a single plate and for the central plate in a cascade of three plates when sAR $=3$ (a), sAR $=1$ (b), and sAR $=0.5$ (c), for the different Re considered.

5. Conclusions

We have analyzed in this work the flow through a cascade of flat plates, measuring in a wind tunnel the lift and drag coefficients as the angle of attack is varied for several, relatively low values of the aspect ratio and the Reynolds number. The comparison of these measurements with those, also obtained here, for the flow on an isolated plate shows, as the main feature, that the lift coefficient for a plate in the cascade has a pronounced maximum when the angle of attack is roughly twice that above which the single plate becomes stalled. An exception is when the aspect ratio of the plates is below unity, in which case the aerodynamic characteristics are quite similar in both cases.

All these results have been obtained in a particular cascade configuration of interest for a device designed to extract hydrokinetic energy from tidal and river currents. The power coefficient in this configuration is shown to be larger than that obtained with an isolated plate only when the aspect ratio is large enough (semispan aspect ratio 3 in this study). This is due to the fact that the drag coefficient is also enhanced in relation to the single plate for the same range of angles of attack where the lift coefficient reaches its pronounced maximum, thus limiting its effect on the power coefficient. Further investigations should be undertaken to obtain the optimal cascade configuration for extracting the maximum power for a given tidal current, considering a wider set of cascade configurations. This has to be done through less expensive numerical simulations, and including the effect of the separation between blades or solidity, of different angles and speeds of the cascade in relation to the current, and using blades with more elaborated profiles than the case of a rectangular flat plate. Part of this numerical work is currently under progress. The present study may serve as an experimental benchmark in which relevant aspects related to the effects of the angle of attack, the aspect ratio and the Reynolds number have been revealed.

Acknowledgments

This work has been supported by the Ministerio de Ciencia e Innovación of Spain, Grant no. ENE2010-16851. Comments by Pedro Mayorga, Technical Director of EnerOcean S.L., are gratefully acknowledged.

References

Buffum, D.H., Fleeter, S., 1991. Wind Tunnel Wall Effects in a Linear Oscillating Cascade. Technical Report TM-103690. NASA.
Gostelow, J.P., 1984. Cascade Aerodynamics. Pergamon Press, Oxford.
Hawthorne, W.R. (Ed.), Aerodynamics of Turbines and Compressors. High Speed Aerodynamics and Jet Propulsion, vol. 10, Princeton University Press, Cambridge, USA
Hodson, H.P., Howell, R.J., 2005. Bladerow interactions, transition, and high-lift aerofoils in low-pressure turbines. Annual Review of Fluid Mechanics 37, 71–98.
Keuthe, A.M., Chow, C.Y., 1997. Foundations of Aerodynamics: Bases of Aerodynamic Design, 5th ed. Wiley, New York.
Mayorga, P., 2012. Technical Director of EnerOcean S.L., private communication.
McLaren, K., Tullis, S., Ziada, S., 2012. Measurement of high solidity vertical axis wind turbine aerodynamic loads under high vibration response conditions. Journal of Fluids and Structures 32, 12–26.
Mueller, T., Kellogg, J., Ifju, P., Shkarayev, S. (Eds.), 2007. Introduction to the Design of Fixed-Wing Micro Air Vehicles, AIAA, Reston.
Pelletier, A., Mueller, T.J., 2000. Low Reynolds number aerodynamics of low-aspect-ratio, thin/flat/cambered-plate wings. Journal of Aircraft 37, 825–832.
'Tidal Sails AS', 2012. ⟨http://tidalsails.com⟩.
Torres, G.E., Mueller, T.J., 2004. Low-aspect-ratio wing aerodynamics at low Reynolds numbers. AIAA Journal 42, 865–873.
Weinig, F.S., 1964. Theory of two-dimensional flow through cascades. In: Hawthorne, W.R. (Ed.), Aerodynamics of Turbines and Compressors. High Speed Aerodynamics and Jet Propulsion, vol. 10. , Princeton University Press, Cambridge, USA, pp. 13–81.
Winter, H., 1936. Flow Phenomena on Plates and Airfoils of Short Span. Technical Report TM 798. NACA.